Human Molecular Genetics, 2017, Vol. 26, No. 9 1643–1655

doi: 10.1093/hmg/ddx069
Advance Access Publication Date: 21 February 2017
Original Article

ORIGINAL ARTICLE

Perturbations in cell signaling elicit early cardiac defects in mucopolysaccharidosis type II

Roberto Costa[1], Andrea Urbani[2], Marika Salvalaio[3,4], Stefania Bellesso[3], Domenico Cieri[5], Ilaria Zancan[1], Mirella Filocamo[6], Paolo Bonaldo[1], Ildiko Szabò[2], Rosella Tomanin[3] and Enrico Moro[1,*]

[1]Department of Molecular Medicine, [2]Department of Biology, [3]Department of Women's and Children's Health, University of Padova, I-35131 Padova, Italy, [4]Pediatric Research Institute "Città della Speranza," I-35127 Padova, Italy, [5]Department of Biomedical Sciences, University of Padova, I-35131 Padova, Italy and [6]Centro di Diagnostica Genetica e Biochimica delle Malattie Metaboliche Istituto Giannina Gaslini, I-16147 Genova, Italy

*To whom correspondence should be addressed at: Department of Molecular Medicine, University of Padova, Via Ugo Bassi 58/B, 35121 Padova, Italy. Tel: +39 498276341; Fax: +39 498276079; Email: moroe@bio.unipd.it

Abstract

Morphogens release and activity can be negatively affected by an impaired glycosaminoglycans (GAGs) turnover and proteoglycans assembly in the extracellular matrix, leading to altered tissue morphogenesis. In this work, we show that loss of Iduronate-2-sulfatase (IDS) activity, affecting GAGs catabolism and responsible for a life-threatening valvulopathy in mucopolysaccharidosis type II (MPSII), triggers early Sonic Hedgehog (Shh) and Wnt/β-catenin signaling defects, leading to aberrant heart development and atrioventricular valve formation in a zebrafish model. In addition, we consistently found impaired Shh signaling activity and cardiac electrophysiological abnormalities in IDS knockout mice at postnatal stages before any evident massive GAGs accumulation. These results suggest that IDS activity substantially affect cardiac morphogenesis through impaired Shh signaling and document an unexplored role of the enzyme in the fine-tuning of cell signaling pathways.

Introduction

Glycosaminoglycans (GAGs) are widely distributed glycopolymers covalently attached to the core protein of proteoglycans (PGs), which are strictly involved in cell homeostasis and tissue plasticity. In the basement membrane, Collagen IV and PGs physically interact and play a fundamental role in structural maintenance and macromolecule interactions during tissue maturation (1,2). However, PGs and sulfated GAGs perform different modulatory activities, which are not related to their structural role. For example, inhibition of the plasma complement activation requires the complement factor H, which binds to heparan sulfate (HS) residues on host cell surfaces (3,4). Moreover, PGs are key components of the cellular glycocalix, which is involved in intercellular communication, and cancer cells displaying a metastatic behavior are often characterized by alterations in the sulfated GAGs pattern (5,6).

GAGs modulate signaling factors and cytokines by enabling the interaction of the ligand(s) with a specific receptor, or by preventing the activity of cytokines and secreted molecules via sequestration (7–10). Similarly, GAGs and related PGs play key roles during embryonic development and cell differentiation, by allowing the correct morphogens diffusion (11). The latter role is particularly relevant in undifferentiated precursor cells, exposed to antagonizing signaling ligands and committed to different cell fates. To achieve the fine-tuning of cell signaling differentiation, GAGs need to restrict the diffusion of

Received: January 31, 2017. **Revised:** January 31, 2017. **Accepted:** February 17, 2017

morphogens towards the correct target cells, in order to elicit a temporally and spatially-regulated tissue specification (12). The wide range of PGs and GAGs functions is related to their intrinsic properties, including: *i)* the large amounts of GAGs building blocks; *ii)* a plethora of possible structural conformations and *iii)* the variable chemical modifications affecting GAGs chain conformation. Among the latter, sulfatation is a reversible modification, which allows a dynamic cellular response and quick extracellular matrix remodelling. Iduronate (Ido) sulfatation is a very common modification of heparan and dermatan sulfate, providing negative charges to GAGs and ultimately contributing to the specific binding of Sonic hedgehog ligands (13).

How impaired GAGs metabolism is involved in pathogenic processes is clearly illustrated by lysosomal storage disorders (LSDs), such as Hunter syndrome (Mucopolysaccharidosis type II, MPSII, OMIM # 309900). MPSII is a rare disorder caused by the deficit of IDS, a lysosomal hydrolase involved in GAGs catabolism (14). Loss of IDS function is associated with a systemic and progressive accumulation of heparan and dermatan sulfates in most tissues and organs (particularly liver, heart, spleen, bones, joints and in the severe forms, also the brain), ultimately leading to several abnormalities, including hepatosplenomegaly, skeletal deformities and valvular heart disease (15). Heart failure is common in MPSII patients and significantly affects their life expectancy, being responsible in many cases to premature death (16,17).

In MPSII patients, GAGs accumulation progressively occurs in the ventricular chamber, aortic lumen and cardiac valves (particularly mitral and aortic ones), contributing to the cardiac impairment and leading to valvular stenosis (18,19). Thus, to allow for extended life expectancy, cardiac valve replacement is often required in severely affected patients (20). Additionally, progressive left ventricular hypertrophy and interventricular septal thickening may further lead to impaired cardiac function (17–19). Heart failure, characterizing most, if not all, Hunter patients, has been often ascribed to the abrogation of IDS enzymatic activity and consequent GAGs accumulation. However, GAGs have also a cryptic regulatory function for several morphogens, including Sonic Hedgehog (Shh), a key signaling factor during heart ontogenesis and cardiac cell regeneration (21,22).

In this work, we provide a proof of concept that cardiac abnormalities in fish and mouse models for MPSII are strongly related to impaired cell signaling activities, including a defective Shh pathway, before any overt GAGs accumulation is detectable. We also demonstrate that a defective heart electrophysiological activity, particularly a prolonged P-R interval, is detectable in IDS knockout mice before any evident massive GAGs storage. We, therefore, disclose a novel pathogenic paradigm, in which well-defined cell signaling alterations trigger early cardiac defects in MPSII.

Results

Loss of IDS function affects Shh signaling during zebrafish development

We previously documented well-defined developmental defects in a transient IDS-deficient zebrafish model obtained by using a translation initiation blocking morpholino ($IDS_{atg}MO$) (23). In the present work, to investigate for molecular pathways specifically affected by IDS deficiency in early development, we microinjected the $IDS_{atg}MO$ into one cell-stage embryos of cell signaling reporter transgenics (CSRs), expressing a fluorescent reporter gene (GFP or mCherry) under the control of responsive elements for different developmental signaling pathways (Wnt, Notch, Shh, BMP, TGFβ) (24). The ability of $IDS_{atg}MO$ to reduce Ids protein levels was confirmed by western blot analysis of multiple independent morphant and control fish lysates (Supplementary Material, Fig. S1).

Among different CSRs, a recently generated Shh reporter transgenic line (25) was clearly affected by Ids loss of function. A significant reduction of GFP expression was detected in whole-mounted 24 hours post fertilization (hpf) Tg(12xGli.HSV:GFP)^{ia11} fish microinjected with the $IDS_{atg}MO$, while reporter activity was unaffected in age-matched larvae microinjected with a mismatch control morpholino (Fig. 1A, upper panels). Similar results were obtained with a different Shh reporter line, Tg(12xGli.HSV:nlsmCherry)^{ia10} (Fig. 1A, lower panels), thus ruling out a preferential sensitivity of the reporter transgene to the morpholino activity. Moreover, multiple microinjections were performed on the offspring from different reporter transgene carriers, thus excluding artefacts due to positional effects (data not shown). Interestingly, the morpholino-dependent decrease of Shh reporter activity was restricted to the first 48 h (Supplementary Material, Fig. S2) and reverted by the co-injection of a human *IDS* mRNA (Figs. 1A–C), thus supporting a direct role of Ids activity in modulating the Shh pathway. Ids deficit did not significantly impair other signaling pathways during the very early stages of zebrafish development (5 to 28 hpf), as revealed by morpholino injection into CSR embryos for either Wnt, Notch, BMP or TGFβ pathways (data not shown), thus suggesting that Shh signaling was preferentially affected by Ids loss of function.

When more deeply evaluating Shh signaling misregulation, we observed reduced reporter expression at 28 hpf in the dorsocephalic regions of morphants heart, when compared with mismatch control fish. Down-regulation of the Shh pathway due to Ids depletion was further confirmed in other body areas, such as the neural tube and caudal regions (Fig. 1D, middle and bottom panels), as revealed by confocal microscopy analysis at high magnification.

Shh is required for primitive heart specification in zebrafish

Zebrafish heart development starts from mesodermal-cells at 5 hpf and involves the timely and spatially-defined specification of myocardial and endocardial precursors (21,26,27). All cardiac developmental steps are under the control of several morphogens, which trigger the differentiation of endocardial and myocardial precursors (28–30). In particular, at 6-somite stage, fish cardiac progenitors express the *hand2* gene (31,32), coding for a transcription factor upstream of the Shh pathway, and, accordingly, arterial and endothelial lineages are committed by a Shh-dependent response. Therefore, although the underlying mechanism is not fully understood and cardiac cells require other stimuli, heart development is severely affected by Shh depletion (21). To assess for a Shh-dependent role in heart development, we administered the Smoothened (Smo) antagonist, cyclopamine (Cya) (33), to Tg(BRE-AAVmlp:EGFP)^{ia18}(24) embryos from 8 to 24 hpf (Fig. 2). At 27 hpf, Cya treated-larvae displayed a primitive heart with a cone shape and defective contractility. Moreover, and in agreement with previous observations (34), angioblasts were reduced and the primitive outflow tract (OFT) was not developed yet (data not shown). Conversely, mock-treated (DMSO 0.1%) larvae displayed a heart with tubular shape and many circulating cells. After Cya withdrawal, all treated fish survived beyond 48 hpf, despite evident heart tube malformations. Therefore, Shh signaling activity is instrumental for the development of the cardiac tissue, and its abrogation for a short window of time during embryogenesis is sufficient to cause permanent heart malformations.

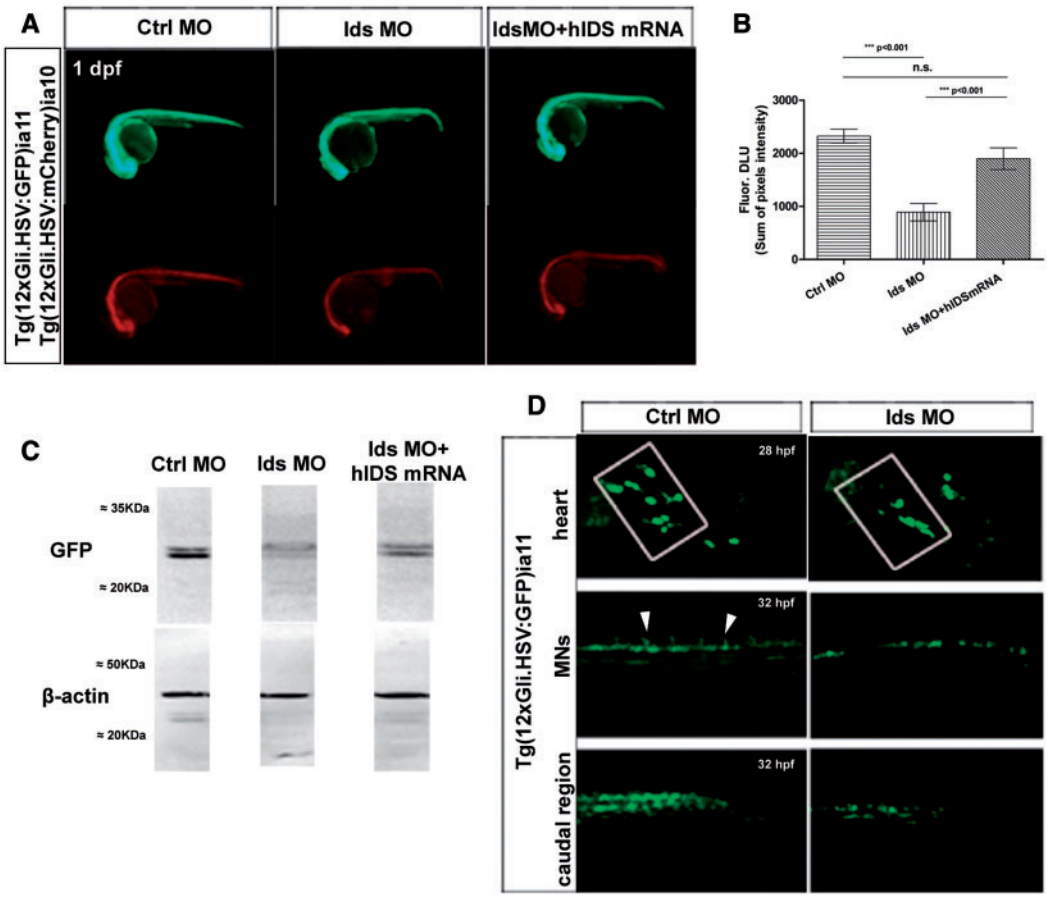

Figure 1. IDS loss of function is associated with Shh pathway defects in zebrafish. **(A)** Representative 1 dpf double Tg(12xGli.HSV:GFP)^{ia11} (upper panel)/ Tg(12xGli.HSV:mCherry)^{ia10} (lower panel) larva, showing the decrease of reporter transgene expression after morpholino-based IDS knockdown and rescued reporter transgene activity after coinjection of $IDS_{atg}MO$ with human *IDS* mRNA (control MO, $N = 140$; $IDS_{atg}MO$, $N = 95$; $IDS_{atg}MO + hIDS$ mRNA, $N = 150$). All images are lateral views, with anterior to the left. **(B)** In silico ImageJ-based quantification of fluorescence intensity of the control, morphant and rescued larvae (control MO, $N = 140$; $IDS_{atg}MO$, $N = 95$; $IDS_{atg}MO + hIDS$ mRNA, $N = 150$). Data are expressed as mean ± SEM for the assayed conditions (***$P < 0.001$; *t*-test). **(C)** Representative Western blot performed on 1 dpf control, rescued and morphant Tg(12xGli.HSV:GFP)^{ia11} larvae, displaying the quantitative decrease of GFP expression in morphant fish when compared with control larvae ($N = 30$ for each condition). **(D)** Confocal Z-stack of a representative 28–32 hpf control MO- and $IDS_{atg}MO$–injected Tg(12xGli.HSV:GFP)^{ia11} fish, showing decreased Shh reporter expression in the heart, trunk and caudal regions. Arrowheads point to the motorneurons (MNs). All images are lateral views, with anterior to the left.

Shh signaling is affected in the heart of IDS knockout mice

To assess whether the dysregulation of the Shh pathway triggered by Ids loss of function in fish was also found in mammalian animal models, we investigated a previously described IDS knockout mouse model (35). Dissected hearts from a total cohort of nine IDS knockout mice and nine wild-type siblings at postnatal stages P7 ($N = 6$ for each condition) and P14 ($N = 3$ for each condition) were subjected to transcriptional and proteomic analysis. qRT-PCR analysis for various targets of the Shh pathway revealed significantly lower Shh and Ptch1 mRNA levels in hearts of IDS knockout mice when compared with age-matched wild-type siblings (Fig. 3A). We also measured transcript levels for genes related to myocardial differentiation and heart function (FoxM1, Ramp1 and Bmp4) and found significantly decreased mRNA levels for BMP4 and FoxM1 in heart samples from IDS knockout mice (Fig. 3A).

To verify whether the decreased levels of Shh pathway-related transcripts were paralleled by reduced protein levels of the same genes, we carried out western blot analysis on protein extracts from dissected hearts of P14 mice. Despite individual knockout mice hearts displayed slight differences, we detected decreased levels of the Shh ligand and Shh transducer, Gli1, in IDS knockout mouse hearts, with respect to the corresponding wild-type control samples. (Fig. 3B). Accordingly, immunofluorescence for Shh and Gli1 on paraffin-embedded hearts of P7 mice revealed a decrease of Shh and Gli-immunopositive cells in IDS knockout mice when compared with wild-type mice (Fig. 3C).

Taken together, these data point at a defective activity of the Shh pathway in the heart of IDS knockout mice. Moreover, the finding that FoxM1 and BMP4 mRNA levels are decreased in IDS knockout hearts suggests that defective Shh pathway activity may be associated with impaired cardiomyocyte differentiation at postnatal stages.

Loss of IDS function affects heart ventricle development and trabeculation in both fish and mouse models

Since BMP4 and FoxM1 mRNAs levels were decreased in heart lysates from IDS knockout mice (Fig. 3A) and the Hedgehog

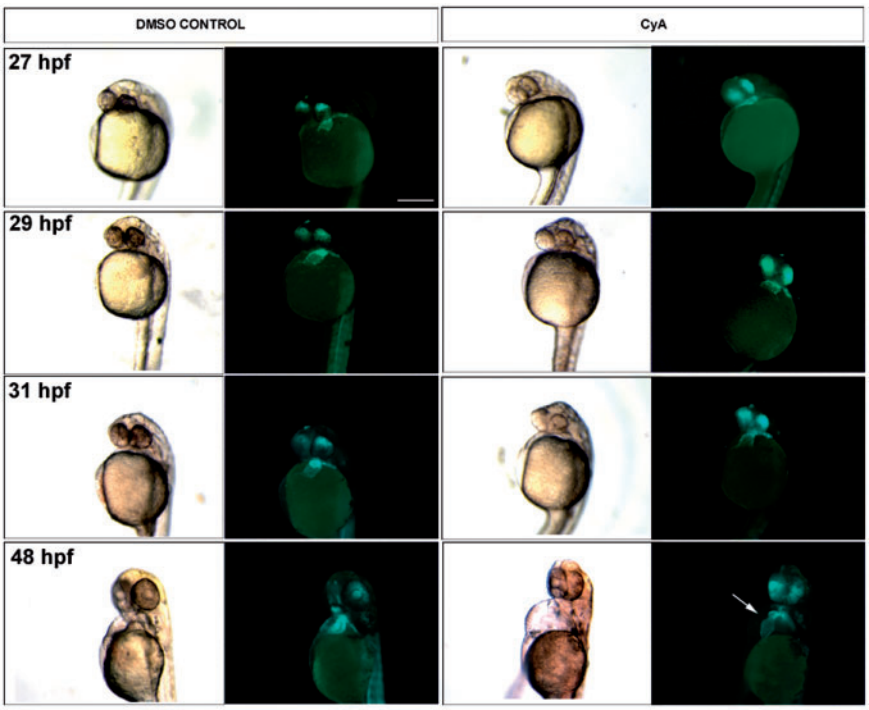

Figure 2. Shh pathway is required for heart development in fish larvae. Representative Tg(BRE-AAVmlp:d2GFP)^{ia18} fish embryos treated with DMSO and 30 μM cyclopamine (CyA) at 8–24 hpf and analyzed at the indicated developmental stages under epifluorescence and visible light. The CyA-induced cardiac malformation is marked by a white arrow. (Fisher exact test, $^{***}P < 0.001$; $N = 40$ for each condition) Scale bar, 0.25 mm.

activity was negatively affected by Ids depletion in zebrafish, we speculated that a primary defect of the cardiomyocyte differentiation program could be associated with abnormal heart chamber morphogenesis in IDS loss of function models. To verify this hypothesis, we first carried out confocal imaging on morphant and control fish larvae at different life stages using as readout the Tg(BRE-AAVmlp:EGFP)^{ia18} line. As shown in Fig. 4A and B, we found that Ids morphant larvae display an impaired cardiac morphogenesis and enlarged atrium when compared with age-matched controls. A detailed confocal analysis of the ventricular chamber, using the Tg(UAS:JAG1)^{el108} line confirmed a marked defect in myocardial trabeculation, as well as a different outflow tract morphology, in Ids morphants (Fig. 4C–E and Supplementary Material, Movie S1–S3). Notably, the impaired cardiac trabeculation in fish morphants persisted also at later life stages (Fig. 4F and G).

We next verified whether IDS knockout mice displayed similar defects in heart chamber morphogenesis. Towards this aim, we carried out serial sections of paraffin-embedded hearts from P60 IDS knockout mice and age-matched wild-type controls. Histological staining revealed reduced myocardial trabeculation in IDS knockout mice, which was reminiscent of the defect observed in morphant fish (Fig. 4H–I). Alcian blue staining of the same sections showed very limited GAG accumulation, suggesting that heart morphogenesis defects may be limitedly affected by GAG storage (Fig. 4J–M). To further evaluate this aspect, we performed Alcian blue staining on paraffin-embedded hearts of P7 and P14 mice, a stage at which we started to detect Shh-related molecular defects. Although we found Alcian blue positivity in the cardiac valve regions of both wild-type and IDS knockout mice in agreement with previous observations (36), we were unable to detect widespread GAGs accumulation in the heart of IDS knockout mice at this age (Supplementary Material, Fig. S3A–F'). The presence of clustered GAGs in the heart valves (both atrioventricular valve and outflow tract) under physiological conditions was also confirmed in wild-type fish at 10 days post fertilization (dpf) (Supplementary Material, Fig. S3G–H).

These findings indicate that absent or reduced IDS function is responsible for impaired cardiac morphogenesis as a consequence of progressive deterioration in heart trabeculation, despite the presence of limitedly localized GAGs.

Cardiac trabeculation defects in Ids morphant fish are rescued by manipulation of the Shh pathway

Since Hedgehog signaling defects have been shown to be associated with decreased *cmlc*-expressing differentiated cardiomyocytes (37), we sought to verify whether the decreased Shh reporter activity in Ids morphants could be responsible for a defective cardiomyocytes specification. To this purpose, we first verified whether Shh reporter-expressing cardiac cells in Tg(12xGli.HSV:mCherry)^{ia10}/Tg(UAS:jag1)^{el108} fish mirror the *cmlc*-expressing cell population. As shown in Fig. 5A and Movie S3, we found that at both 3 dpf and 6 dpf *cmlc*-expressing cells are co-labeled by the Shh reporter transgene. We next evaluated whether by promoting the ectopic activation of the Shh pathway using the Smoothened agonist Purmorphamine (PuA) (38) we could recover the trabeculation defects in Ids morphants. Towards this aim, we provided morphant fish with a pulse of PuA in a restricted window of time, before cardiac chamber morphogenesis. As shown in Figure 5B, by PuA treatment we were able to partially rescue the ventricle trabeculation defect in morphants.

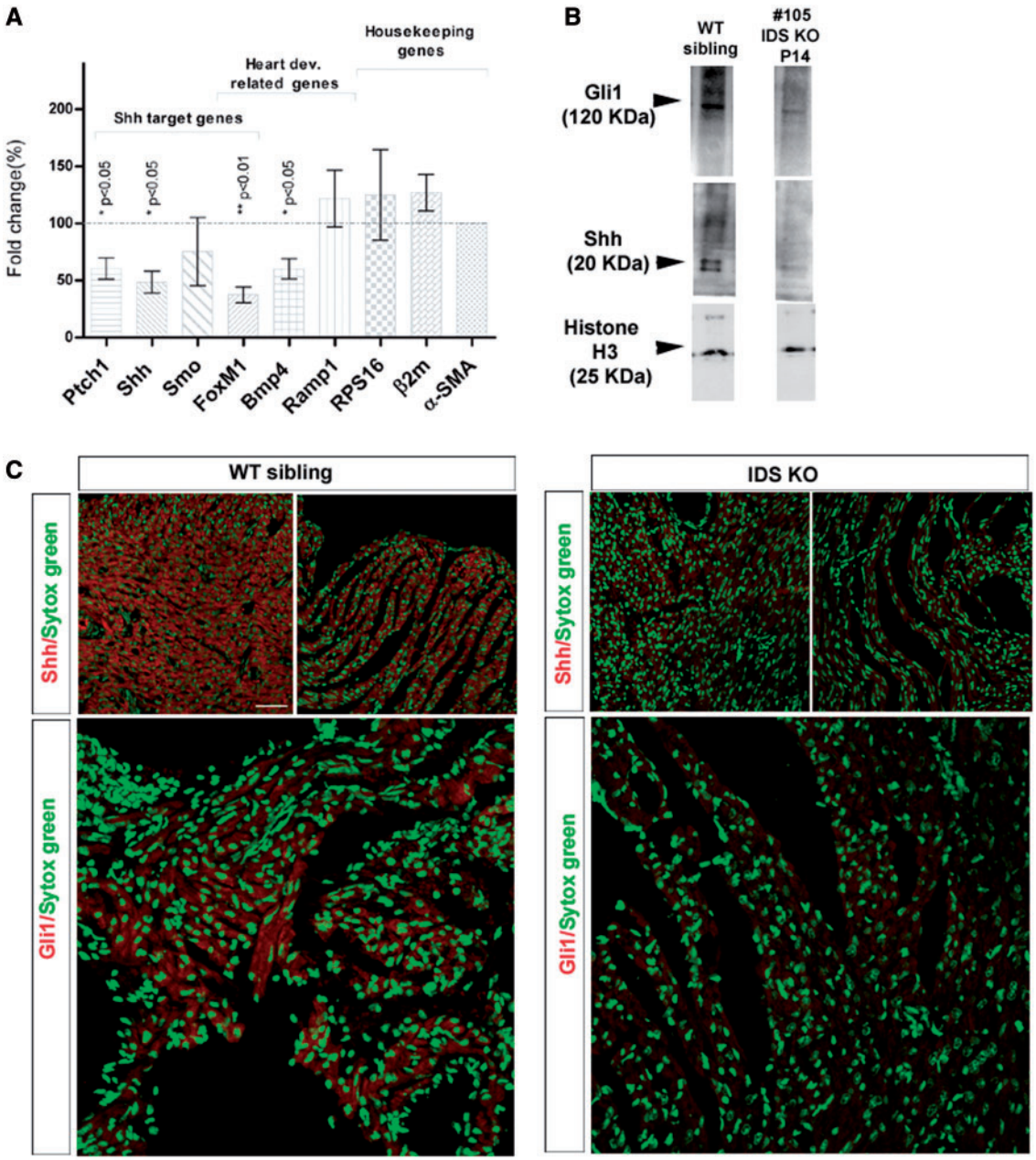

Figure 3. IDS knockout mice display Shh pathway defects in the heart. **(A)** Bar-graph of qRT-PCR analysis for Shh pathway-related and housekeeping genes in isolated hearts of P7 mice ($N = 3$, wild-type; $N = 3$ IDS knockout mice). Normalized fold expression levels for each gene are shown using α−actin for normalization and ribosomal RNA s16 and beta-2 microglobulin as calibrators (*$P < 0.05$;**$P < 0.01$; *t*-test). **(B)** Representative western blot for Gli1 and Shh is isolated hearts from a P14 IDS knockout mouse. Pooled hearts from age-matched wild-type siblings were used as control. H3 Histone was used as a loading control ($N = 3$ for both wild-type and IDS knockout hearts). **(C)** Representative immunostaining for Shh and Gli1 in paraffin-embedded hearts of P7 IDS knockout mice ($N = 3$) and age-matched wild-type siblings ($N = 3$), showing reduced Shh and Gli1 immunoreactivity in IDS knockout mice. Nuclear sytox-green was used as counterstaining.

Therefore, we could conclude that cardiomyocytes specification appears to be negatively affected by Ids loss of function and ectopic activation of the Shh pathway can partially prevent the onset of trabeculation defects in fish morphants.

Increased Wnt/β-catenin signaling in IDS morphant fish is associated with impaired atrioventricular canal differentiation

Wnt/β-catenin is a pleiotropic pathway, which tightly interacts with the Shh pathway by a bidirectional feedback mechanism, leading to cellular proliferation and differentiation (39). Impaired canonical Wnt signaling has been often associated with valvular defects in several cardiac disorders (40,41), suggesting that the fine tuning of this pathway is fundamental for heart valve development. To evaluate whether Ids loss of function, besides impairing the Shh pathway, was also affecting the canonical Wnt signaling, we carried out several experiments by testing the $IDS_{atg}MO$ on the previously generated zebrafish Wnt reporter line, Tg(7xTCFX.lasiam:mCherry)^{ia5} (42). At 72 hpf, Wnt reporter activity evaluated by *in situ* hybridization was enhanced in the atrioventricular canal (AVC) and in the outflow

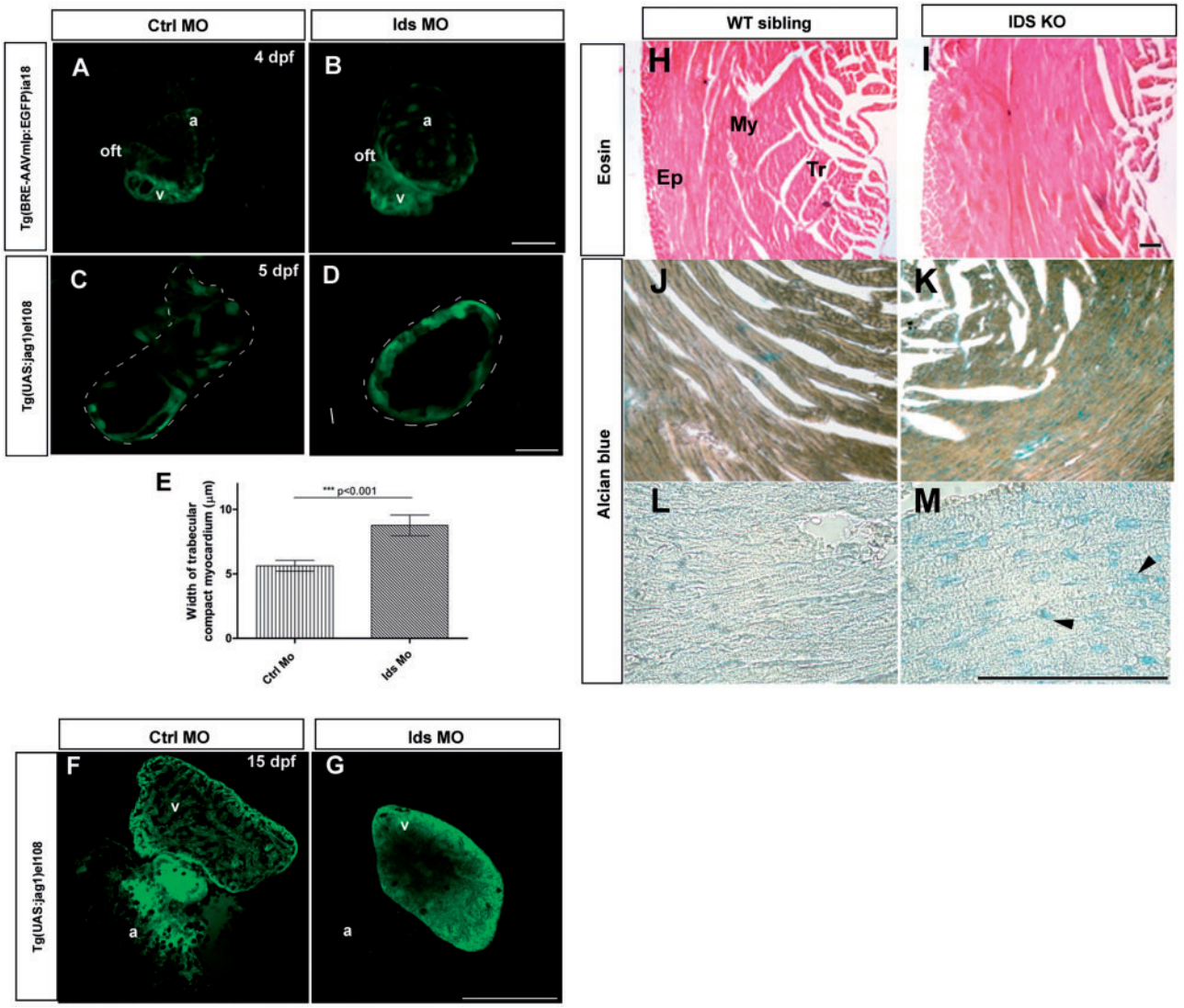

Figure 4. Impaired heart morphogenesis and cardiac trabeculation defects occur in IDS loss of function fish and mouse models. **(A, B)** Representative confocal Z-stack projection, showing the atrial enlargement detected in 4dpf Tg(BRE-AAVmlp:d2GFP)^{ia18} morphant larvae (B) when compared with age-matched controls (A) (Fisher exact test, $^{**}P < 0.01$ $N = 1$ out of 60 for control and $N = 11$ out of 44 for morphants). Scale bar, 50 μm. **(C, D)** Representative confocal Z-stack projection of a ventricle section, from 5 dpf Tg(UAS:jag1)^{el108} control and morphant fish, showing the increased thickness of the compact myocardium (white small bar) and the reduced trabeculation occurring in morphants. The dotted line depicts the overall area of the ventricle in which all measurements have been performed. Scale bar, 20 μm **(E)** Bar-graph, showing the increased compact myocardium thickness detected in Ids morphants. Data are expressed as mean ± SEM of 30 measurements performed in 10 animals for each condition. (t-test, $^{**}P < 0.001$). **(F, G)** Representative confocal Z-stack projections of a 15 dpf Tg(UAS:jag1)^{el108} control (F) and morphant fish (G), showing the persistent impaired ventricle trabeculation occurring in morphants. $N = 5$ for each condition. a: atrium; v: ventricle. **(H, I)** Eosin-stained histological sections of dissected hearts of P60 wild-type and IDS knockout mice ($N = 3$ for each condition), showing altered trabeculation and heart structure as a consequence of IDS loss of function. **(J–M)** Alcian blue-stained sections from dissected hearts of P60 wild-type and IDS knockout mice, showing the progressive GAGs deposition at the heart level in IDS knockout mice. K and L are high magnification of the mycocardial region in wild-type and IDS knockout mice, respectively. Scale bar, 50 μm. a, atrium; avc, atrioventricular canal; Ep: epicardium; MY: myocardium oft, outflow tract; Tr trabeculae; v, ventricle.

tract of fish morphants when compared with age-matched controls (Fig. 6A and B). Confocal analysis using the alternative Wnt reporter line, Tg(7xTCFXla.siam:EGFP)^{ia4}, showed increased transgene expression in morphants at higher morpholino dose and only at 5 dpf, probably as a consequence of the long half-life of the reporter protein (Fig. 6C–E). The effects on the Wnt reporter transgene were no longer evident after 5 dpf, probably due to the restricted temporal activity of the morpholino (Fig. 6E).

To evaluate whether the enhanced Wnt reporter activity due to the transient Ids morpholino action together with Shh pathway deregulation could be potentially involved in prolonged heart valve structural defects, we carried out whole mount confocal microscopy analysis in isolated hearts from 30 dpf Ids morphants and age-matched mismatch controls. As shown in Fig. 6F and G, while at this stage in mismatch control fish the cardiac AVC had four leaflets and a circular morphology, Ids morphants displayed a disorganization of the AVC.

Since the morphogenesis of the AVC in morphants can be influenced by mechanical forces and blood flow (43), we examined cardiac parameters, including the cardiac volume and shortening fraction. As shown in Figure 6H, we did not detect any evident functional abnormality. Moreover, live imaging and confocal analysis on double Tg(UAS:JAG1)^{el108}/Tg(gata1:DsRed)

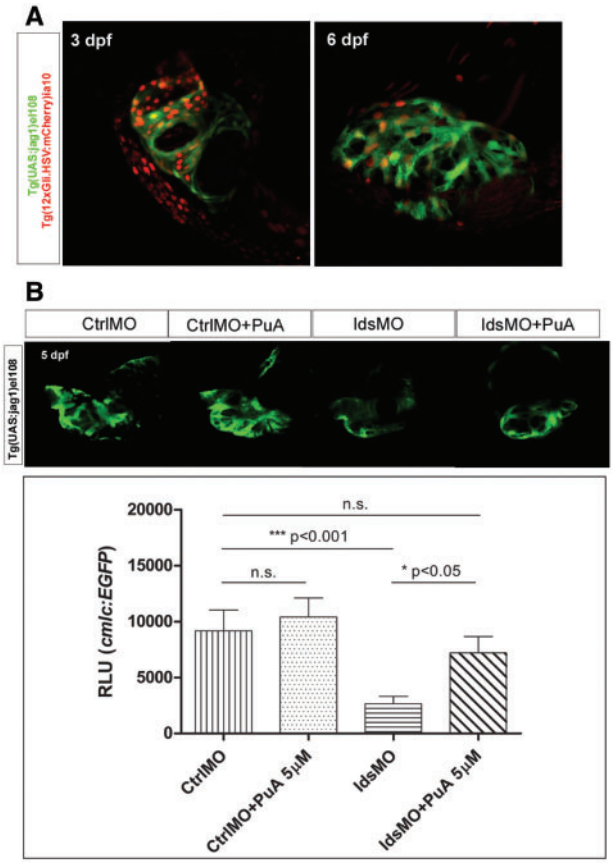

Figure 5. Shh-dependent myocardial trabeculation defects in Ids morphants are partially rescued by Purmorphamine (PuA) treatment. **(A)** Representative confocal Z-stack projection of the ventricle from 3 dpf and 6 dpf Tg(12xGli.HSV:mCherry)^{ia10}/Tg(UAS:jag1)^{el108} fish, showing the colocalization of Shh reporter-expressing nuclei with cmlc-expressing cardiomyocytes. **(B)** (upper panel) Representative confocal Z-stack projections of the ventricular trabeculation from 5 dpf Tg(UAS:jag1)^{el108} control fish and morphants with or without PuA treatment. (lower panel) Bar-graphs showing the quantitative analysis of cardiac trabeculation recovery after PuA treatment. Data are expressed as mean ± SEM of 10 larvae for each condition. Scale bar, 50 µm.

fish did not further show particular blood flow defects occurring in morphants when compared with age-matched controls (Supplementary Material, Movie S4).

These findings reveal that Ids depletion leads to increased activity of the canonical Wnt pathway, which, in the absence of evident cardiac functional defects, could explain the aberrant morphogenesis of the AVC at late life stages.

Electrophysiological analysis of IDS knockout mice reveals an early-onset defective heart conductance

Based on the signaling dysregulation and heart morphogenesis defects triggered by IDS depletion in fish and mouse models, we speculated that the heart activity of IDS deficient animals could be affected during early life stages, when GAGs accumulation was still limited. Electrocardiogram (ECG) recordings were performed under isoflurane anesthesia in 1-month-old IDS knockout mice and wild-type control littermates. Among different cardiac parameters (P wave, QRS interval, PR interval and QT interval), we found that the PR interval was significantly prolonged in 1-month-old IDS knockout mice, when compared with age-matched wild-type mice (Fig. 7A). Moreover, P wave duration was also different between wild-type and IDS knockout mice, although the difference was not barely statistically significant ($P = 0.0526$). In particular, in two out of eight IDS knockout mice, we detected a marked prolonged PR, which resembled a characteristic atrioventricular block (Supplementary Material, Fig. S4). All values are summarized in Table 1. To better characterize the PR interval lengthening, we analyzed time-dependent variations of the following parameters: RR, PR, QRS and QT intervals. As expected, we found a slow, but progressive, anesthesia-dependent RR lengthening during the experiment, with no QRS or QT lengthening (44). Conversely, PR contribution to RR duration increase seemed to be relevant, both in wild-type and in IDS knockout mice. We thus analyzed PR/QT ratio over the time in every experiment, and found a statistically significant increased average steepness of the fitting line in IDS knockout mice (wild-type: 0.00303 ± 0.00015; IDS knockout: 0.00824 ± 0.00012, $P < 0.001$) (Fig. 6B). Moreover, two out of eight knockout mice showed a non-linear PR/QT increase over time (data not shown); interestingly, these animals were the ones which displayed the apparent atrioventricular block during the recording time. We then explored whether the heart performance defects were also displayed at later life stages, by repeating ECG recordings on the same cohorts after 1 month. Unlike 1-month-old, 2-month-old IDS knockout mice did not show any statistically significant difference when compared with age-matched wild type control sibling for each ECG parameter. However, PR/QT overtime kinetics were still different between wild-type and IDS knockout mice, as the steepness of the PR/QT ratio kinetic was 0.00159 ± 0.00019 for wild-type and 0.00706 ± 0.00014 for IDS knockout mice ($P < 0.001$). These data indicate that IDS ablation leads to lengthened cardiac PR-interval during early postnatal life, when GAGs accumulation is still limited.

Discussion

Heart functional impairment is one of the most debilitating aspects of MPSII, which may contribute to the high morbidity and mortality of patients affected by mucopolysaccharidosis type II (17,45). Despite the improvement of systolic ventricular function, the progression of cardiac valve thickening and dysfunction does not appear to be prevented in patients subjected to enzyme replacement therapy (ERT), underlining the need of targeted complementary therapies. Previous studies have emphasized the detrimental role of GAGs accumulation in the onset of heart valve defects and cardiac abnormalities (16). However, a clear pathogenetic mechanism linking the progressive GAGs accumulation to the onset of mitral valve regurgitation and heart failure is still missing. Moreover, the traditional concept that organs dysfunction in LSDs can be ascribed to substrate accumulation has been challenged by recent findings, supporting the scenario in which lysosomal impairment is tightly associated with defects of the autophagic machinery and extracellular matrix remodelling, which may drive LSD disease symptoms (46,47).

By using two different animal models for MPSII, we disclosed a novel pathogenic mechanism underlying heart functional impairment, which relies on a complex cascade of signaling defects occurring in different heart cell lineages, leading to defective cardiac tissue patterning and differentiation. We documented a decreased activity of the Shh pathway in both mouse and zebrafish MPSII models, which is consistent with a deficient endocardial and myocardial differentiation program, in

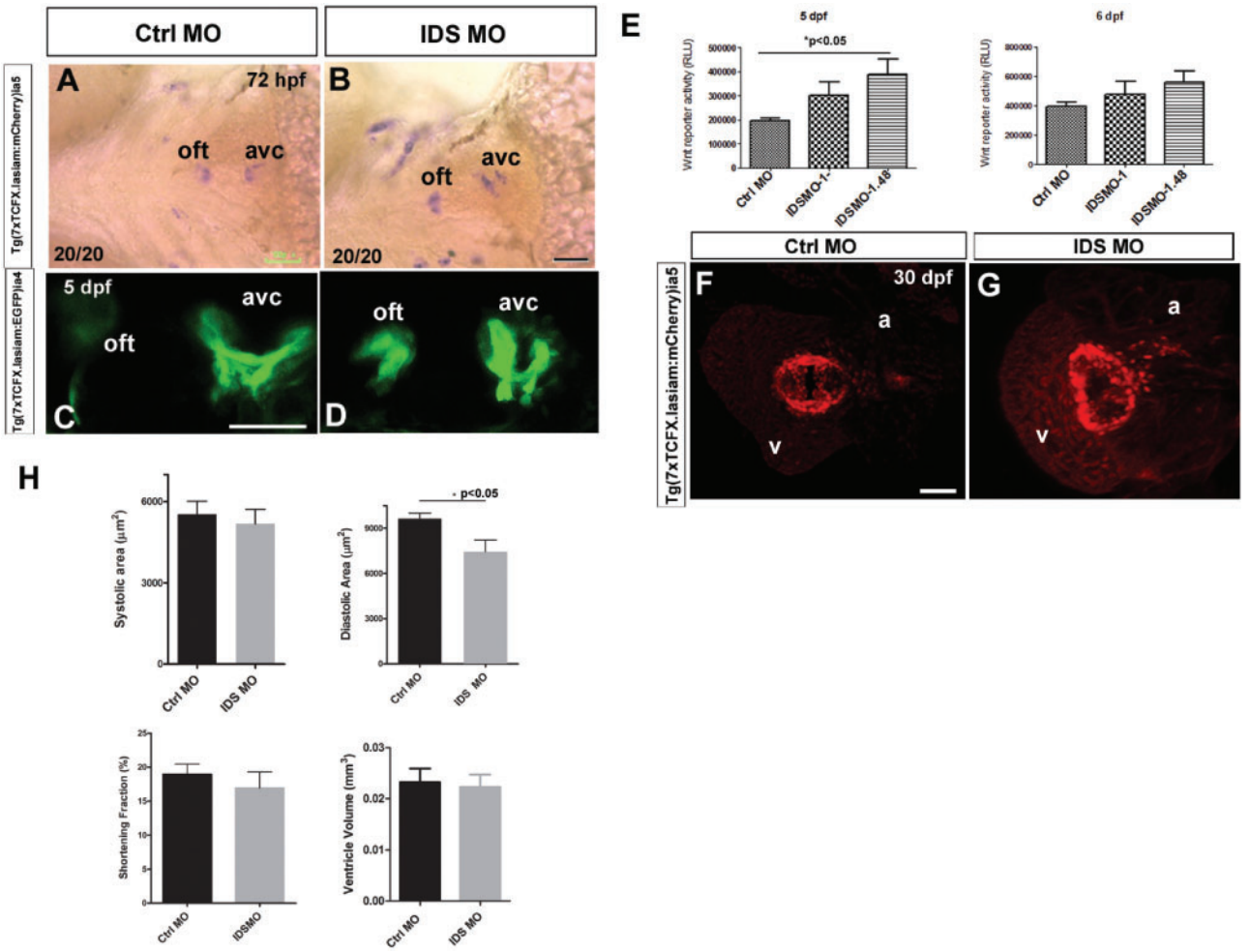

Figure 6. Canonical Wnt signaling pathway is dysregulated in heart valves of IDS fish morphants. **(A, B)** Representative ventral view of Tg(7xTCFX.lasiam:mCherry)^{ia5}control and morphant larvae analyzed by *in situ* hybridization at 3 dpf, showing upregulation of the canonical Wnt signaling in the atrioventricular canal and outflow tract of morphants. (Fisher exact test, $^{***}P < 0.001$, $N = 20$ for each condition) Scale bar, 100 μm. **(C, D)** Representative confocal Z-stack projection of the atrioventricular canal (avc) and outflow tract (oft) from a 5 dpf Tg(7xTCFX.lasiam:EGFP)^{ia4} control and morphant larva, showing the increased Wnt reporter activity in the two cardiac structures occurring in morphants Scale bar, 25 μm. **(E, F)** Bar-graphs showing the quantitative detection of the Wnt signaling reporter activity in the atrioventricular canal. (t-test; $P < 0.05$; $N = 5$ larvae for each condition) (F, G) Representative confocal Z-stack projection of a 30 dpf Tg(7xTCFX.lasiam:mCherry)^{ia5} morphant and control larva showing the abnormal heart valve morphology in morphant fish (Fisher exact test, $^{***}P < 0.01$, $N = 20$ for each condition). Scale bar, 100 μm. **(H)** Bar-graphs, showing the functional parameters, including the systolic area, the diastolic area, shortening fraction and ventricle volume measured in 4 dpf Tg(UAS:JAG1)^{el108}/Tg(gata1:DsRed) control and morphant fish. Data are expressed as mean±SEM of three independent measurements performed in six animals for each condition (t-test; $^{*}P < 0.05$).

agreement with previous observations (7,30). The identification of disrupted Shh signaling as a consequence of IDS loss of function during early life stages represents a novelty in the field of congenital heart defects associated with LSDs. Moreover, our findings support the well-known concept that GAGs play a key role in Shh modulation. Indeed, GAGs-dependent regulation of Shh transduction was clearly described by using *in vitro* and *in vivo* models (37), and our data not only represent a further *in vivo* evidence of this close functional association, but they are also the first demonstration of the role of this axis in in the cardiac pathogenesis of GAGs-related LSDs (Mucopolysaccharidoses and Mucolipidoses).

Together with a defective Shh pathway, we detected a significantly overactive Wnt/β-catenin signaling in the heart valves of Ids knockdown fish during early larval stages, which was associated with progressive loss of myocardial trabeculation and enlarged atrium development. On the other hand, when assessing cardiac functional parameters, including the shortening fraction, no evident abnormalities were distinguishable in fish morphants. Considering that the mechanosensitive endocardial signalling (i.e. Klf2) may indirectly affect the Wnt signalling and cardiac valve development (43) we do not rule out that it may affect cardiac valves during late life stages. However, since the increase in Wnt/β-catenin signalling was observed in morphants during the first days of cardiac development, when we did not detect functional abnormalities, we speculate that the effect may be due to the transient morpholino-mediated Ids loss of function, rather than a disrupted mechanosensitive pathway.

In IDS knockout mice at postnatal stages, we detected the same trabeculation defect together with FoxM1 and BMP4 down-regulation and defective heart electrophysiology, i.e. prolonged P-R interval. Interestingly, canonical Wnt signaling was shown to be required for the proper AVC patterning and

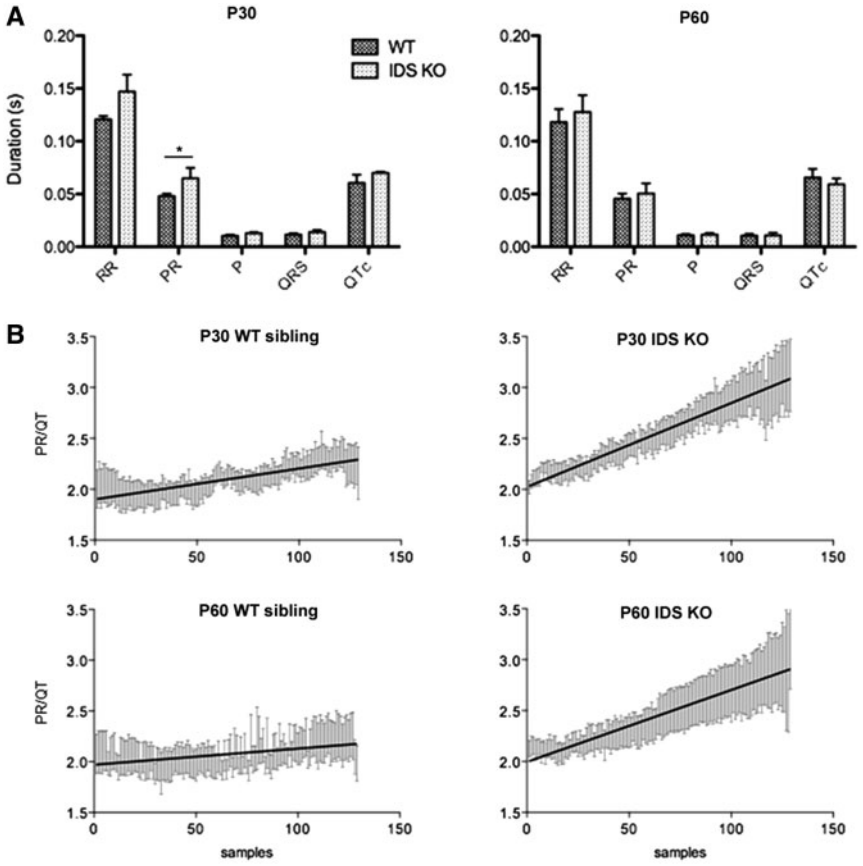

Figure 7. Prolonged PR interval is detected in IDS knockout mice. **(A)** Average RR interval, PR interval, P wave duration, QRS complex duration and QTc from wild-type ($N = 6$) and IDS knockout mice ($N = 8$) at 1 month and 2 months of age. Error bars represent SD (*, $P < 0.01$, KW test). **(B)** Average overtime PR/QT kinetics (linear fitting + SEM) from wild-type and IDS knockout mice at 1 month and 2 months of age. In the X-axis, the progressive number of heartbeat measurements (corresponding to 20 heartbeats for each value) is depicted as samples.

Table 1. Average RR interval, PR interval, P wave duration, QRS complex duration, QT interval, QTc, and PR/QT from wild-type and IDS knockout mice at 1 month and 2 months of age; Avg: average; bmp: beats per minute; s: seconds; SD: standard deviation

	Condition				WT			
Age								
1 month	RR (s)	HR (bpm)	PR (s)	P (s)	QRS (s)	QT (s)	QTc (s)	PR/QT
Avg	0,121	498	0,048	0,01	0,011	0,021	0,061	2,17
SD	0,003	13	0,002	0,001	0,001	0,003	0,008	0,236
2 months	**RR (s)**	**HR (bpm)**	**PR (s)**	**P (s)**	**QRS (s)**	**QT (s)**	**QTc (s)**	**PR/QT**
Avg	0,118	513	0,046	0,011	0,01	0,022	0,065	2,059
SD	0,012	48	0,005	0,001	0,002	0,003	0,008	0,362
	Condition				**IDS KO**			
Age								
1 month	**RR (s)**	**HR (bpm)**	**PR (s)**	**P (s)**	**QRS (s)**	**QT (s)**	**QTc (s)**	**PR/QT**
Avg	0,147	412	0,065	0,013	0,014	0,027	0,07	2,642
SD	0,016	43	0,01	0,001	0,002	0,001	0,001	0,507
2 months	**RR (s)**	**HR (bpm)**	**PR (s)**	**P (s)**	**QRS (s)**	**QT (s)**	**QTc (s)**	**PR/QT**
Avg	0,128	477	0,051	0,011	0,011	0,021	0,059	2,444
SD	0,016	50	0,01	0,002	0,003	0,002	0,005	0,491

cardiac electrical programming (40). Given that in the transient morpholino-based loss of function fish model an overtly altered heart valve patterning is detected at later life stages, it is conceivable that the early postnatal window of time required for the Wnt pathway-mediated AVC maturation is critical to the proper leaflet formation and heart valve function. Moreover, patients affected by the Ebstein anomaly, a congenital heart disease, occurring in infants of pregnant women under treatment with LiCl (a known Wnt pathway agonist), are at high risk of developing a prolonged P-R interval and AV block, a key ECG

anomaly that we detected in IDS knockout mice at postnatal stages (48). We cannot explain why the prolonged PR interval was seen just at 1 month, while at two months it became not significantly different between IDS KO mice and age-matched wild-type siblings. We speculate that in the early stages of cardiac pathophysiology compensatory mechanisms may be triggered to reduce the burden of cardiac dysfunction. Nevertheless, in both IDS KO mice and human patients irreversible cardiac function worsening occurs at late life stages.

Taken together, although our data cannot imply that Shh and Wnt signaling defects are the only primary pathogenic mechanism of congenital heart disease in MPSII patients, the localized GAGs storage in heart valves during physiological conditions together with minimal or limitedly detectable GAGs accumulation in heart myocardium of IDS knockout mice at postnatal stages support the view that lysosomal and extracellular GAGs accumulation leading to valvular stenosis and histiocyte infiltration might not be considered the only primary pathomechanism.

In contrast to other LSDs, in which the phenotypic abnormalities are less severe and limited to few organs in affected patients (e.g. MPSIII/Sanfilippo syndrome) (49), the single enzymatic deficit in MPSII is associated with a broad spectrum of organ defects, resulting in a complex phenotype, which can range from attenuated to severe. This may emphasize a key role for the IDS protein, not only as a catabolizing enzyme but also as a key signaling hub with a subtle tuning activity towards relevant cell processes (i.e. differentiation).

Our work provides also support to the view that early diagnosis in Hunter patients is relevant, theoretically allowing patients to gain access to the treatment as early as possible, thus potentially slowing down the disease progression and the occurrence of precocious and irreversible signs and symptoms. It remains to be verified whether patients would completely benefit from an ERT started immediately after birth, concerning their heart pathology. Nonetheless, in agreement with a recent overview (50) and, given the complex nature of LSDs, it is plausible to take into account the application of combined therapies, in addition to ERT. In this context, the identification of cell signaling alterations upstream of the substrate storage defect, as demonstrated in this work, may pave the way for the development of additional novel targeted therapies.

Materials and Methods

Zebrafish lines and mice

Fish housing was carried out at 28.5 °C according to standard rules and procedures (https://zfin.org). Tg(BRE-AAVmlp:EGFP)^{ia18} carries an EGFP reporter transgene under the control of BMP responsive elements (24). Tg(UAS:JAG1)^{el108} express a cmlc2:EGFP transgene in the heart (51).

IDS knock-out mice and wild type were expanded in animal facility and housed in light and temperature controlled conditions, with food and water provided ad libitum. Murine IDS knock out have been previously described (35). All animal manipulation procedures were conducted according to the Local Ethical Committee at the University of Padua and National Agency (Italian Ministry of Health).

Morpholino injection and validation

IDS functional knockdown was obtained using the previously described morpholino (23). In rescue experiments, MO-injected embryos were randomly separated and injected with 10 nl of a solution containing the morpholino plus 17 ng/μl of the purified mRNA for human IDS.

Cyclopamine and purmorphamine treatment

Cyclopamine hydrate (Calbiochem, Merck, Milan, Italy) was dissolved in DMSO and partially dechorionated embryos were incubated with a 30 μM Cya, beginning at 8 hpf. Cyclopamine treatment was stopped at 24 hpf by replacing with fresh medium. After five washes, embryos were then mounted and analyzed by fluorescence microscopy.

For rescue experiments fish were treated with Purmorphamine (Sigma, Italy) from 10 hpf to 18 hpf at 5 μM concentration. After several washes with fresh medium fish were raised up to 5 dpf and evaluated under confocal microscopy.

GAGs staining in whole mount zebrafish and mouse heart

Embryos were fixed in 4% buffered p-formaldehyde in PBS o/n and washed for 15 min for three times in Alcian blue buffer (ABB) (50 mM glycine, 3% acetic acid, pH 2.5). Deparaffinized slides from mouse samples and whole-mount hearts were stained with a 1% Alcian blue solution in ABB for 30 min, and then washed in ABB for 30 min. Stained samples were mounted and photographed with a LeicaM165FC. Counterstaining was performed with eosin or Nuclear Fast red (Sigma, Milan, Italy).

Immunostaining

Immunlabeling was performed according to standard procedures. Briefly, deparaffinized heart slides were washed several times with PBT (PBS, 0.01% Tween) and blocked with 3% goat serum (Thermofisher, Milan, Italy) and 0.03% TritonX100 for 2 h. Incubation with primary antibodies was done overnight at 4 °C, and after several washes immunostaining was achieved with fluorescently-tag secondary antibodies. Primary antibodies against Gli1 (#2534; Cell Signaling Biotechnology, Danvers, USA), Shh (SC9024; Santa Cruz Biotechnology, Dallas, USA), H3 histone (AB1791; Abcam, Cambridge, UK) were used at 1:100 dilution. TRITC and and FITC-conjugated secondary antibodies (Thermofisher, Milan, Italy) were incubated at 1:500 dilution. Counterstaining was performed with 5 mM Sytox-green (Thermofisher, Milan, Italy) at 1:10000 dilution.

Microscopy and image acquisition

Zebrafish embryos expressing fluorescent proteins were analyzed using a Leica M165FC epifluorescent microscope. All pictures were acquired with a Nikon DS-F12 digital camera. Confocal zebrafish images were acquired with a Nikon C2 H600L confocal microscope, while mouse slices were acquired with Leica DMR compound/Nomarski microscope. All images were acquired with the same exposure parameters and processed *in silico* with Gimp1 and Adobe Photoshop.

For cardiac morphology and shortening fraction measurements, fish at 5 dpf were analyzed under confocal microscopy and images processed by ImageJ software (https://imagej.nih.gov/ij/).

All parameters have been assessed according to the protocol described by Hoage and colleagues (52).

Real time PCR

All murine hearts were homogeneized by glass dounce in Trizol reagent (Thermofisher, Milan, Italy) and total RNA was isolated according to the manufacturer's protocol. RNAs were resuspended in 80 μl of RNAse free water and then quantified by Nanodrop 1000 spectrofotometer. A total of 5 μg of total RNAs was reverse-transcribed by SuperScriptIII kit (Thermofisher, Milan, Italy). Purified cDNAs were subjected to quantitative real-time PCR using Rotorgene 3000 instrument and Syber green (Thermofisher, Milan, Italy). Primers are listed in Supplementary Material, Table 1. Cts were extrapolated by data transformation using real-time plots, Cts of α-SMA were used as cDNAs quantitative standard. Relative gene expression among samples was normalized using the comparative ct method. Three biological replicates were used for each condition, while six experimental replicates were performed for each biological sample. Differennt housekeeping genes were used for data standardization (α-SMA) and as internal controls (RPS16, β2m).

Western blot

Fish larvae and murine heart protein lysates were prepared using a lysis buffer (50 mM Tris/HCl, pH 7.5, 150 mM NaCl, 0.02% NP-40) supplemented with protease inhibitor (Roche Diagnostics, Mannheim, Germany) and Phosphatase Inhibitor Cocktails 2 and 3 (Sigma-Aldrich, Milan, Italy). Samples homogeneization were performed by a glass dounce. The lysates were centrifuged at 13 000 × g for 30 min at 4 °C. The supernatant was collected and protein concentration was determined by the Bradford method. Extracted proteins were supplemented with 4x sample buffer, heated at 70 °C for 5 min and run onto precast SDS-PAGE (Thermofisher, Milan, Italy). Proteins were transferred on Immobilon-P membranes (Merk Millipore, Italy) in 25 mM Tris, 192 mM glycine, 20% methanol (v/v), 0.1% SDS. Membranes were incubated overnight with primary antibodies against the following proteins: Shh (SC9024; Santa Cruz Biotechnology, Dallas, USA), H3 histone (AB1791; Abcam, Cambridge, UK), β-actin (SC59459; Santa Cruz Biotechnology, Dallas, USA), Gli1 (#2534; Cell signaling Biotechnology, Danvers, USA), IDS (003423A01; ABnova, Taipei, Taiwan), GFP (SC9996; Santa Cruz Biotechnology,Dallas,USA). All antibodies were used at 1:1000 diluition. HRP Chemiluminescence signals were detected by Kodak Image Station 4000MMpro (Eastman Kodak, New Haven, CT) and analyzed with the Kodak Image software.

ECG analysis

ECG was performed under inhalation anesthesia conditions, and each mouse was anesthetized by a mixture of isofluorane and oxygen delivered by inhalation with a mask. Once anesthesia induction was assessed by observation of the paw-withdrawal reflex suppression, two small needles were inserted subcutaneously in the mouse anterior paws (explorative electrodes) and one in the posterior left one (reference electrode). ECG signals using the explorative electrodes were detected by a PowerLab 8/35 (ADInstruments), and acquired by LabChart 7 Pro software (ADInstruments) at a frequency of 10 kHz, with no filters. ECG was performed for 5 min to increase the chance of detecting functional abnormalities, while heartbeat was maintained at a physiologic rate. Recordings were analyzed with LabChart 7 Pro software (ADInstruments): single heartbeats were detected every 20 heartbeats and averaged to minimize eventual artifacts and noise, and every average was processed semi-automatically to identify single ECG waves. The following parameters were considered: P wave and QRS complex duration, intervals between P wave and QRS complex establishment (PR interval) and between Q wave and T wave (QT interval). To perform the normalization, we measured also the RR interval, as it underlies the instantaneous heartbeat frequency. QT interval was corrected for the heartbeat frequency, by means of the Bazett's formula ($QTc = QT/(RR)^{1/2}$), leading to a corrected QT interval (QTc). All parameters are expressed as mean and SD; statistical difference was tested by means of Kruskal-Wallis' analysis of variance. Overtime kinetics of RR, PR, QRS, and QT intervals were analyzed, together with the PR/QT ratio. PR/QT overtime kinetics were averaged and linearly fitted for both cohorts; the resultant linear fittings were compared between the two cohorts and tested for statistical significance with Fisher's test.

Supplementary Material

Supplementary Material is available at *HMG* online.

Acknowledgements

We thank Dr Martina Milanetto and Dr Luigi Pivotti for excellent fish husbandry assistance.

Conflicts of Interest statement. None declared.

Funding

This work has been partly financially supported by the Italian Ministry of Health (Ricerca Finalizzata GR-2008-1139743) to E.M.

References

1. Timpl, R., Wiedemann, H., van Delden, V., Furthmayr, H. and Kuhn, K. (1981) A network model for the organization of type IV collagen molecules in basement membranes. *Eur. J. Biochem.*, **120**, 203–211.
2. Yurchenco, P.D., Tsilibary, E.C., Charonis, A.S. and Furthmayr, H. (1986) Models for the self-assembly of basement membrane. *J. Histochem. Cytochem.*, **34**, 93–102.
3. Schmidt, C.Q., Herbert, A.P., Kavanagh, D., Gandy, C., Fenton, C.J., Blaum, B.S., Lyon, M., Uhrin, D. and Barlow, P.N. (2008) A new map of glycosaminoglycan and C3b binding sites on factor H. *J. Immunol.*, **181**, 2610–2619.
4. Loeven, M.A., Rops, A.L., Berden, J.H., Daha, M.R., Rabelink, T.J. and van der Vlag, J. (2015) The role of heparan sulfate as determining pathogenic factor in complement factor H-associated diseases. *Mol. Immunol.*, **63**, 203–208.
5. Linhardt, R.J. and Toida, T. (2004) Role of glycosaminoglycans in cellular communication. *Acc. Chem. Res.*, **37**, 431–438.
6. Basappa, K.S. and Rangappa, K. (2014) Sugahara, Roles of glycosaminoglycans and glycanmimetics in tumor progression and metastasis. *Glycoconj. J.*, **31**, 461–467.
7. Whalen, D.M., Malinauskas, T., Gilbert, R.J. and Siebold, C. (2013) Structural insights into proteoglycan-shaped Hedgehog signaling. *Proc. Natl. Acad. Sci. USA*, **110**, 16420–16425.
8. Sterner, E., Meli, L., Kwon, S.J., Dordick, J.S. and Linhardt, R.J. (2013) FGF-FGFR signaling mediated through glycosaminoglycans in microtiter plate and cell-based microarray platforms. *Biochemistry*, **52**, 9009–9019.

9. Bulow, H.E. and Hobert, O. (2006) The molecular diversity of glycosaminoglycans shapes animal development. *Annu. Rev. Cell Dev. Biol.*, **22**, 375–407.
10. Coombe, D.R. (2008) Biological implications of glycosaminoglycan interactions with haemopoietic cytokines. *Immunol. Cell Biol.*, **86**, 598–607.
11. Nguyen, T.K., Tran, V.M., Sorna, V., Eriksson, I., Kojima, A., Koketsu, M., Loganathan, D., Kjellen, L., Dorsky, R.I., Chien, C.B. and Kuberan, B. (2013) Dimerized glycosaminoglycan chains increase FGF signaling during zebrafish development. *ACS Chem. Biol.*, **8**, 939–948.
12. Allen, B.L., Filla, M.S. and Rapraeger, A.C. (2001) Role of heparan sulfate as a tissue-specific regulator of FGF-4 and FGF receptor recognition. *J. Cell Biol.*, **155**, 845–858.
13. Witt, R.M., Hecht, M.L., Pazyra-Murphy, M.F., Cohen, S.M., Noti, C., van Kuppevelt, T.H., Fuller, M., Chan, J.A., Hopwood, J.J., Seeberger, P.H. and Segal, R.A. (2013) Heparan sulfate proteoglycans containing a glypican 5 core and 2-O-sulfoiduronic acid function as Sonic Hedgehog co-receptors to promote proliferation. *J. Biol. Chem.*, **288**, 26275–26288.
14. Wraith, J.E., Scarpa, M., Beck, M., Bodamer, O.A., De Meirleir, L., Guffon, N., Meldgaard Lund, A., Malm, G., Van der Ploeg, A.T. and Zeman, J. (2008) Mucopolysaccharidosis type II (Hunter syndrome): a clinical review and recommendations for treatment in the era of enzyme replacement therapy. *Eur. J. Pediatr.*, **167**, 267–277.
15. Schwartz, I.V., Ribeiro, M.G., Mota, J.G., Toralles, M.B., Correia, P., Horovitz, D., Santos, E.S., Monlleo, I.L., Fett-Conte, A.C., Sobrinho, R.P. *et al.* (2007) A clinical study of 77 patients with mucopolysaccharidosis type II. *Acta Paediatr.*, **96**, 63–70.
16. Braunlin, E.A., Harmatz, P.R., Scarpa, M., Furlanetto, B., Kampmann, C., Loehr, J.P., Ponder, K.P., Roberts, W.C., Rosenfeld, H.M. and Giugliani, R. (2011) Cardiac disease in patients with mucopolysaccharidosis: presentation, diagnosis and management. *J. Inherit. Metab. Dis.*, **34**, 1183–1197.
17. Kampmann, C., Beck, M., Morin, I. and Loehr, J.P. (2011) Prevalence and characterization of cardiac involvement in Hunter syndrome. *J. Pediatr.*, **159**, 327–331 e322.
18. Dangel, J.H. (1998) Cardiovascular changes in children with mucopolysaccharide storage diseases and related disorders–clinical and echocardiographic findings in 64 patients. *Eur. J. Pediatr.*, **157**, 534–538.
19. Mohan, U.R., Hay, A.A., Cleary, M.A., Wraith, J.E. and Patel, R.G. (2002) Cardiovascular changes in children with mucopolysaccharide disorders. *Acta Paediatr.*, **91**, 799–804.
20. Bhattacharya, K., Gibson, S.C. and Pathi, V.L. (2005) Mitral valve replacement for mitral stenosis secondary to Hunter's syndrome. *Ann. Thorac. Surg.*, **80**, 1911–1912.
21. Dyer, L.A. and Kirby, M.L. (2009) Sonic hedgehog maintains proliferation in secondary heart field progenitors and is required for normal arterial pole formation. *Dev. Biol.*, **330**, 305–317.
22. Wang, J., Cao, J., Dickson, A.L. and Poss, K.D. (2015) Epicardial regeneration is guided by cardiac outflow tract and Hedgehog signaling. *Nature*, **522**, 226–230.
23. Moro, E., Tomanin, R., Friso, A., Modena, N., Tiso, N., Scarpa, M. and Argenton, F. (2010) A novel functional role of iduronate-2-sulfatase in zebrafish early development. *Matrix Biol.*, **29**, 43–50.
24. Moro, E., Vettori, A., Porazzi, P., Schiavone, M., Rampazzo, E., Casari, A., Ek, O., Facchinello, N., Astone, M., Zancan, I. *et al.* (2013) Generation and application of signaling pathway reporter lines in zebrafish. *Mol. Genet. Genom.*, **288**, 231–242.
25. Corallo, D., Schiavinato, A., Trapani, V., Moro, E., Argenton, F. and Bonaldo, P. (2014) Emilin3 is required for notochord sheath integrity and interacts with Scube2 to regulate notochord-derived Hedgehog signals. *Development*, **140**, 4594–4601.
26. Keegan, B.R., Feldman, J.L., Begemann, G., Ingham, P.W. and Yelon, D. (2005) Retinoic acid signaling restricts the cardiac progenitor pool. *Science*, **307**, 247–249.
27. Bruneau, B.G. (2013) Signaling and transcriptional networks in heart development and regeneration. *Cold Spring Harb Perspect. Biol.*, **5**, a008292.
28. Rochais, F., Mesbah, K. and Kelly, R.G. (2009) Signaling pathways controlling second heart field development. *Circ. Res.*, **104**, 933–942.
29. Kalogirou, S., Malissovas, N., Moro, E., Argenton, F., Stainier, D.Y. and Beis, D. (2014) Intracardiac flow dynamics regulate atrioventricular valve morphogenesis. *Cardiovasc. Res.*, **104**, 49–60.
30. Wong, K.S., Rehn, K., Palencia-Desai, S., Kohli, V., Hunter, W., Uhl, J.D., Rost, M.S. and Sumanas, S. (2012) Hedgehog signaling is required for differentiation of endocardial progenitors in zebrafish. *Dev. Biol.*, **361**, 377–391.
31. Schoenebeck, J.J., Keegan, B.R. and Yelon, D. (2007) Vessel and blood specification override cardiac potential in anterior mesoderm. *Dev. Cell.*, **13**, 254–267.
32. Galli, A., Robay, D., Osterwalder, M., Bao, X., Benazet, J.D., Tariq, M., Paro, R., Mackem, S. and Zeller, R. (2010) Distinct roles of Hand2 in initiating polarity and posterior Shh expression during the onset of mouse limb bud development. *PLoS Genet.*, **6**, e1000901.
33. Chen, J.K., Taipale, J., Cooper, M.K. and Beachy, P.A. (2002) Inhibition of Hedgehog signaling by direct binding of cyclopamine to Smoothened. *Genes Dev.*, **16**, 2743–2748.
34. Gering, M. and Patient, R. (2005) Hedgehog signaling is required for adult blood stem cell formation in zebrafish embryos. *Dev. Cell*, **8**, 389–400.
35. Garcia, A.R., Pan, J., Lamsa, J.C. and Muenzer, J. (2007) The characterization of a murine model of mucopolysaccharidosis II (Hunter syndrome). *J. Inherit. Metab. Dis.*, **30**, 924–934.
36. Kruithof, B.P., Krawitz, S.A. and Gaussin, V. (2007) Atrioventricular valve development during late embryonic and postnatal stages involves condensation and extracellular matrix remodeling. *Dev. Biol.*, **302**, 208–217.
37. Thomas, N.A., Koudijs, M., van Eeden, F.J., Joyner, A.L. and Yelon, D. (2008) Hedgehog signaling plays a cell-autonomous role in maximizing cardiac developmental potential. *Development*, **135**, 3789–3799.
38. Sinha, S. and Chen, J.K. (2006) Purmorphamine activates the Hedgehog pathway by targeting Smoothened. *Nat. Chem. Biol.*, **1**, 29–30.
39. Ouspenskaia, T., Matos, I., Mertz, A.F., Fiore, V.F. and Fuchs, E. (2016) WNT-SHH Antagonism Specifies and Expands Stem Cells prior to Niche Formation. *Cell*, **164**, 156–169.
40. Gillers, B.S., Chiplunkar, A., Aly, H., Valenta, T., Basler, K., Christoffels, V.M., Efimov, I.R., Boukens, B.J. and Rentschler, S. (2015) Canonical wnt signaling regulates atrioventricular junction programming and electrophysiological properties. *Circ. Res.*, **116**, 398–406.
41. Hermans, K.C. and Blankesteijn, W.M. (2015) Wnt Signaling in Cardiac Disease. *Compr. Physiol.*, **5**, 1183–1209.
42. Moro, E., Ozhan-Kizil, G., Mongera, A., Beis, D., Wierzbicki, C., Young, R.M., Bournele, D., Domenichini, A., Valdivia, L.E., Lum, L. *et al.* (2012) In vivo Wnt signaling tracing through a transgenic biosensor fish reveals novel activity domains. *Dev. Biol.*, **366**, 327–340.

43. SteedBoselli, E.F. and Vermot, J. (2016) Hemodynamics driven cardiac valve morphogenesis. *Biochim. Biophys. Acta*, **1863**, 1760–1766.
44. Tanaka, M. and Nishikawa, T. (1999) Sevoflurane speeds recovery of baroreflex control of heart rate after minor surgical procedures compared with isoflurane. *Anesth. Analg.*, **89**, 284–289.
45. Patel, P., Suzuki, Y., Maeda, M., Yasuda, E., Shimada, T., Orii, K.E., Orii, T. and Tomatsu, S. (2014) Growth charts for patients with Hunter syndrome. *Mol. Genet. Metab. Rep.*, **1**, 5–18.
46. Settembre, C., Fraldi, A., Rubinsztein, D.C. and Ballabio, A. (2008) Lysosomal storage diseases as disorders of autophagy. *Autophagy*, **4**, 113–114.
47. Heppner, J.M., Zaucke, F. and Clarke, L.A. (2015) Extracellular matrix disruption is an early event in the pathogenesis of skeletal disease in mucopolysaccharidosis I. *Mol. Genet. Metab.*, **114**, 146–155.
48. Osiro, S., Tiwari, K.J., Mathenge, N., Rodriguez, J.R., Tubbs, R.S. and Loukas, M. (2013) When lithium hurts: a look at Ebstein anomaly. *Cardiol. Rev.*, **21**, 257–263.
49. Lamanna, W.C., Lawrence, R., Sarrazin, S. and Esko, J.D. (2011) Secondary storage of dermatan sulfate in Sanfilippo disease. *J. Biol. Chem.*, **286**, 6955–6962.
50. Vitner, E.B., Platt, F.M. and Futerman, A.H. (2010) Common and uncommon pathogenic cascades in lysosomal storage diseases. *J. Biol. Chem.*, **285**, 20423–20427.
51. Zuniga, E., Stellabotte, F. and Crump, J.G. (2010) Jagged-Notch signaling ensures dorsal skeletal identity in the vertebrate face. *Development*, **137**, 1843–1852.
52. Hoage, T., Ding, Y. and Xu, X. (2012) Quantifying cardiac functions in embryonic and adult zebrafish. *Methos Mol. Biol.*, **843**, 11–20.